Gravity Governs Shear Localization in Confined Dense Granular Flows

M. Reza Shaebani,[1,*] János Török,[2] Maniya Maleki,[3] Mahnoush Madani,[3] Matt Harrington,[4] Allyson Rice,[5] and Wolfgang Losert[6]

[1] *Department of Theoretical Physics and Center for Biophysics, Saarland University, 66123 Saarbrücken, Germany*
[2] *MTA-BME Morphodynamics Research Group, Department of Theoretical Physics, Budapest University of Technology, and Economics, Budapest H-1111, Hungary*
[3] *Department of Physics & Optics Research Center, Institute for Advanced Studies in Basic Sciences, Zanjan 45137-66731, Iran*
[4] *Department of Physics and Astronomy, University of Pennsylvania, Philadelphia, Pennsylvania 19104, USA*
[5] *Department of Biophysics Institute, UT Southwestern Medical Center, Dallas, TX 75390, USA*
[6] *Department of Physics, University of Maryland, College Park, Maryland 20742, USA*

Prediction of flow profiles of slowly sheared granular materials is a major geophysical and industrial challenge. Understanding the role of gravity is particularly important for future planetary exploration in varying gravitational environments. Using the principle of minimization of energy dissipation, and combining experiments and variational analysis, we disentangle the contributions of the gravitational acceleration and confining pressure on shear strain localization induced by moving fault boundaries at the bottom of a granular layer. The flow profile is independent of the gravity for geometries with a free top surface. However, under a confining pressure or if the sheared layer withstands the weight of the upper layers, increasing gravity promotes the transition from closed shear zones buried in the bulk to open ones that intersect the top surface. We show that the center position and width of the shear zone and the axial angular velocity at the top surface follow universal scaling laws when properly scaled by the gravity, applied pressure, and layer thickness. Our finding that the flow profiles lie on a universal master curve opens the possibility to predict the quasistatic shear flow of granular materials in extraterrestrial environments.

Superficial layers of many planets and asteroids are covered by granular materials that range in size from dust and sand to gravel and boulder [1]. These layers result from several processes, such as volcanic activity, fragmentation, and erosion, and extend to variable depths. Although mechanical behavior of granular matter in low-gravity conditions has recently attracted attention [2–7], it is generally unclear how various geological processes that occur in near-surface granular layers of celestial bodies depend on the gravitational acceleration g. Particularly, the localization of shear in a slow granular flow can initiate more catastrophic phenomena such as avalanches, earthquakes and faulting [8–10]. Despite intensive studies on how and where strain is localized in shear zones [11–22], the mechanism of shear band formation in slow granular flows (thus the role of g) cannot be described by a strain-stress constitutive law, as the flow profile and stress are independent of the shear rate. However, it is crucial to predict the shear flow of granular matter in varying gravitational environments to understand the evolution of planetary and asteroid surfaces and for a successful design of planetary and asteroid exploration programs and operation of landers, rovers, and sub-surface sampling devices.

In granular flows created by slowly shearing the boundaries, the strain often localizes in narrow regions of the order of a few particle diameters near the moving boundary [12, 13]. Nevertheless, wide shear zones can also be created when a shear fracture [23] propagates in the bulk away from the boundaries, and the sides of the fault move past each other in deep layers— the process that is of particular importance in geology; see Fig. 1 for an example of a circular fault line in the bulk. In experiments, wide shear zones have been generated by pinning the shear band in the bottom of Couette geometries far from the cylinder wall [19–22]. The position and horizontal extent of the resulting shear zone have shown power-law scalings with the height H of the pile [19, 20]; the zone evolves towards the axis of cylinder and grows wider as it takes the advantage of the gravity to reach the top surface. However, a transition occurs in the flow structure from shear zones that intersect the top surface to closed ones buried in the bulk as H is further increased [18, 21, 22, 24].

While decreasing gravity insignificantly influences the flow profile near walls [3, 7], the profile away from the boundaries was shown to be sensitive to the choice of g for soft particles [25]. Upon varying g in shearing of rigid particles, one expects that the shear rheology of packings without a constraining top boundary would not be affected as g only rescales the pressure gradient [18]; in contrast, under a confining pressure or if the sheared layer withstands the weight of upper layers, the relative pressure difference between successive horizontal layers of grains depends on g, suggesting that the gravity alters the shear flow profile in this case.

We combine numerical analysis and experiments to explore the role of gravitational acceleration g in slow shear flows of granular materials. We consider a rotating circular fault at the bottom of a horizontally infinite granular layer under confining pressure P_{ext} (Fig. 1) and derive the

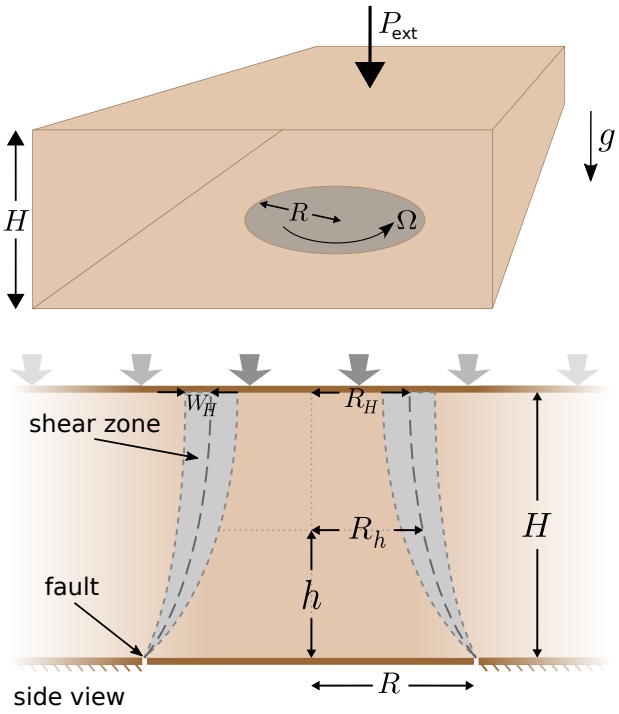

FIG. 1. Sketch of the shear localization zone created by the rotation of a circular region at the bottom of a granular pile. The shear zone reaches the top surface of relatively shallow layers if the external pressure $P_{\rm ext}$ is much weaker than the mean hydrostatic pressure $\frac{1}{2}\rho g H$ induced by gravity; otherwise the zone is buried in the bulk.

shape of the shear localization zone from the variational principle of least energy dissipation [18, 24]. Increasing gravity extends the open shear zone regime to thicker layers and pushes the zone away from the axis of rotation while slightly decreases its width. For closed shear zones, a stronger gravity pulls the shear zone towards the top surface and increases the extent of it. Although the flow profile is controlled by both g and $P_{\rm ext}$, we verify that they are not interchangeable and show that the position and width of the shear zone and the axial angular velocity at the top surface lie on universal master curves when properly scaled by g, H, and $P_{\rm ext}$. We also carry out experiments in a Couette cell geometry to validate the numerical findings. Our results enable us to predict the shear flow profile in slow granular flows for a given set of filling height, confining pressure, and gravitational acceleration.

RESULTS

Shear flow profile from energy dissipation minimization. In order to clarify the role of gravity on the strain localization in sheared granular matter, we consider a shear band initiated by a rough disk with radius R rotated at angular velocity Ω at the bottom of a horizontally infinite granular layer of height H as shown in Fig. 1 (becoming two infinite half-plates moving past each other in the limit $R\to\infty$). Here we assume the same effective friction coefficients in the bulk and near the boundaries, thus, the flow profile remains independent of the choice of μ (though, in general, friction plays a major role in stress transmission in granular materials [26–29]). To describe the flow profile, we apply the principle of least dissipation proposed by Onsager for irreversible time-independent phenomena [30–32]. The validity of this variational approach has been previously confirmed by accurately predicting the strain localization path in various sheared granular systems [16–18, 24, 33–35].

We require a stationary flow that minimizes the rate of energy dissipation and matches the boundary constraints. Denoting the radial coordinate of the shear band at height h with R_h and taking the cylindrical symmetry of the geometry into account, the variational problem is traced back to finding an optimal R_h function that satisfies $R_0{=}R$ while the other boundary at $h{=}H$ is free. In the narrow shear band approximation [18], the dissipation rate is given by the shear stress $\sigma_{\rm tn}=\mu\left(\rho\, g\,(H{-}h){+}P_{\rm ext}\right)$ times the sliding velocity between the two sides $R_h\,\Omega$ integrated over the whole shear band. For the shear stress along the yielding surface we use Coulomb friction between two sliding bodies and assume that the Janssen effect plays no role due to the continuous agitations induced by collisions and slip events which causes a slight creep in the system. Up to a constant prefactor, the expression to be minimized can be formulated as

$$\int_0^H R_h^2\,\sqrt{1{+}\Big(\frac{{\rm d}R_h}{{\rm d}h}\Big)^2}\,\Big(1{-}\frac{h}{H}{+}\frac{P_{\rm ext}}{\rho\, g\, H}\Big)\,{\rm d}h=\min, \qquad (1)$$

thus, the optimal path is generally determined by g, $P_{\rm ext}$, H, and R. Yet, the variational approach predicts that the path is independent of g and $P_{\rm ext}$ and solely determined by H and R in two extreme limits: For a very weak gravity or strong $P_{\rm ext}$, $1\ll\frac{P_{\rm ext}}{\rho\, g\, H}$ and the fabric is isotropic under the homogeneous pressure [36]. In this regime, equation (1) reduces to $\int_0^H R_h^2\,\sqrt{1{+}(\frac{{\rm d}R_h}{{\rm d}h})^2}\,{\rm d}h{=}\min$, which leads to $h{=}\int_R^{R_h}\frac{{\rm d}r}{\sqrt{r^4/A^2{-}1}}$ by solving the Euler-Lagrange equation (A is a constant). The solution can be expressed in terms of the hypergeometric function ${}_2F_1$ as $h{=}r\sqrt{r^4/A^2{-}1}\,{}_2F_1(\frac{3}{4},1;\frac{5}{4};r^4/A^2)$ with the boundary condition $r(h{=}0){=}R$. On the other hand, in the extreme limit of strong gravity or if $P_{\rm ext}\to0$ (as for a layer with a free surface), $\frac{P_{\rm ext}}{\rho\, g\, H}\ll1$ and the strong pressure gradient leads to the variational problem $\int_0^H R_h^2\,\sqrt{1{+}(\frac{{\rm d}R_h}{{\rm d}h})^2}\,(1{-}\frac{h}{H})\,{\rm d}h{=}\min$ [18], which is again independent of g and $P_{\rm ext}$.

The above optimization procedure leads to an instantaneous narrow shear band. However, the material strength is practically affected in the vicinity of yield events [37]

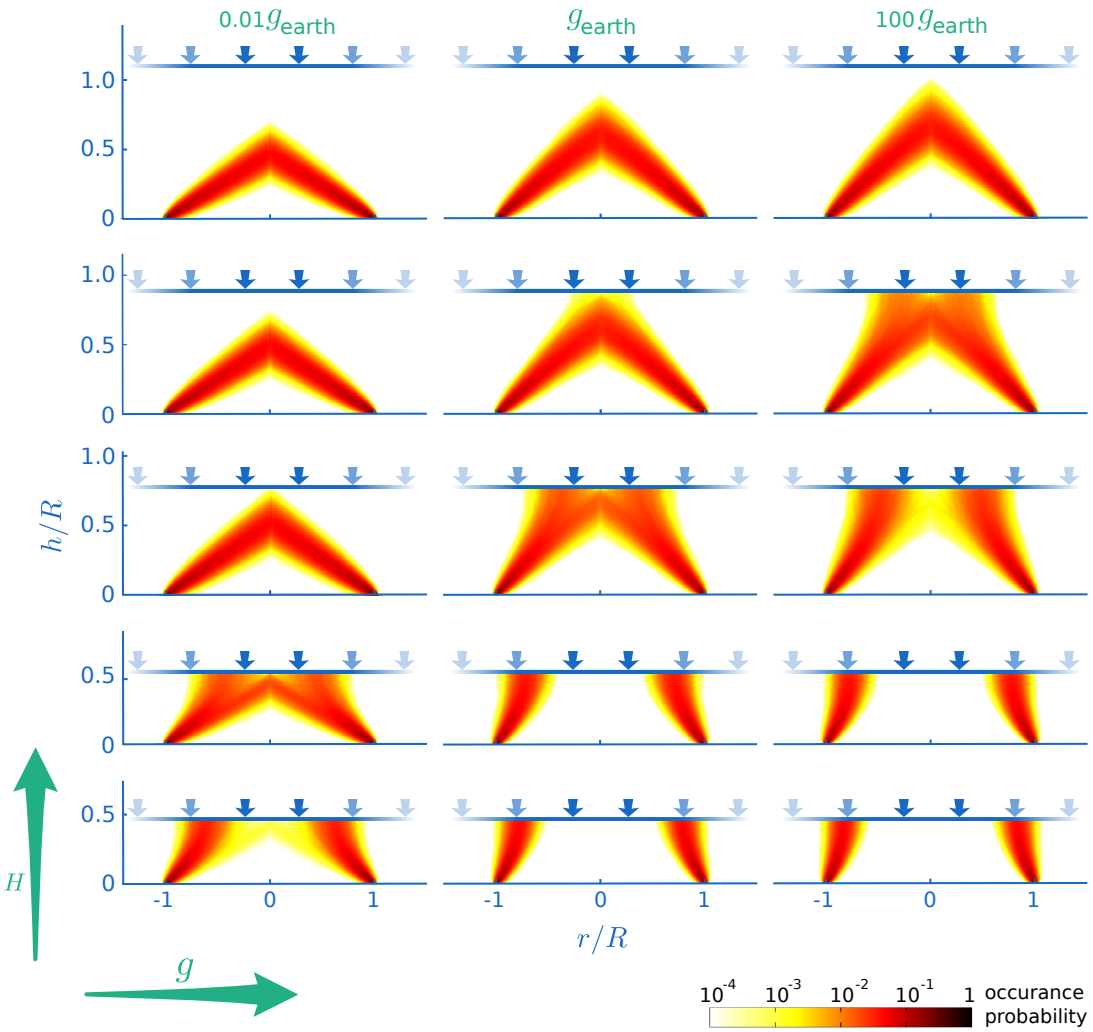

FIG. 2. Dependence of the shear-zone type on gravitational acceleration and filling height. The filling height is H/R=0.48, 0.55, 0.77, 0.88 and 1.10 from the bottom to top row, respectively. The gravitational acceleration in left, middle, and right panels is $\widetilde{g}\equiv g/g_{\text{earth}}$=0.01, 1 and 100, with g_{earth} being the surface gravity of the earth. In all panels, P_{ext} equals the reference pressure $P_\circ$; see main text. The color identifies the occurrence probability at the given point. Open, closed, and combined shear zones can be distinguished.

and the resulting random structural changes slightly vary the minimal path in the next instance. In a fluctuating-band version of the model [24], we introduce local fluctuations of the path around the current shear band (see *Methods* section for details). The resulting shear zone gains a finite width in the course of such a self-organized process where the global optimum path itself modifies the medium in which the optimization is carried out. We obtain the shear profile by ensemble averaging over all instantaneous shear bands calculated via the optimization equation (1) for a given geometry H/R and a set of g and P_{ext} parameters.

Gravity governs the strain localization profile. We perform extensive numerical simulations based on the optimization scheme to clarify the individual roles of H, g and P_{ext} on the shear flow profile as they affect the variational problem differently; H influences both the integral limit and integrand in equation (1). Also, g and P_{ext} impose a pressure gradient or an isotropic pressure, respectively, thus they are not interchangeable factors.

In case of a free top surface, i.e. P_{ext}=0, we checked that the flow profile is controlled by H/R [18–20] and that gravity plays no role. However, the strength of the pressure gradient induced by g is expected to influence the flow profile for $P_{\text{ext}}, \neq 0$ since an isotropic confining pressure changes the micro-structure and dilation behavior of the material [7, 25, 38–41]. To verify this expectation, we fix the applied pressure at a nonzero value and vary g by several orders of magnitude at different values of H (For ease of comparison, we introduce a reference pressure level $P_\circ$ that a pile with height H/R=0.1 consisting of glass beads of size d applies on the bottom disk with R/d=100 in the gravitational acceleration of the earth g_{earth}). Interestingly, by increasing the gravity,

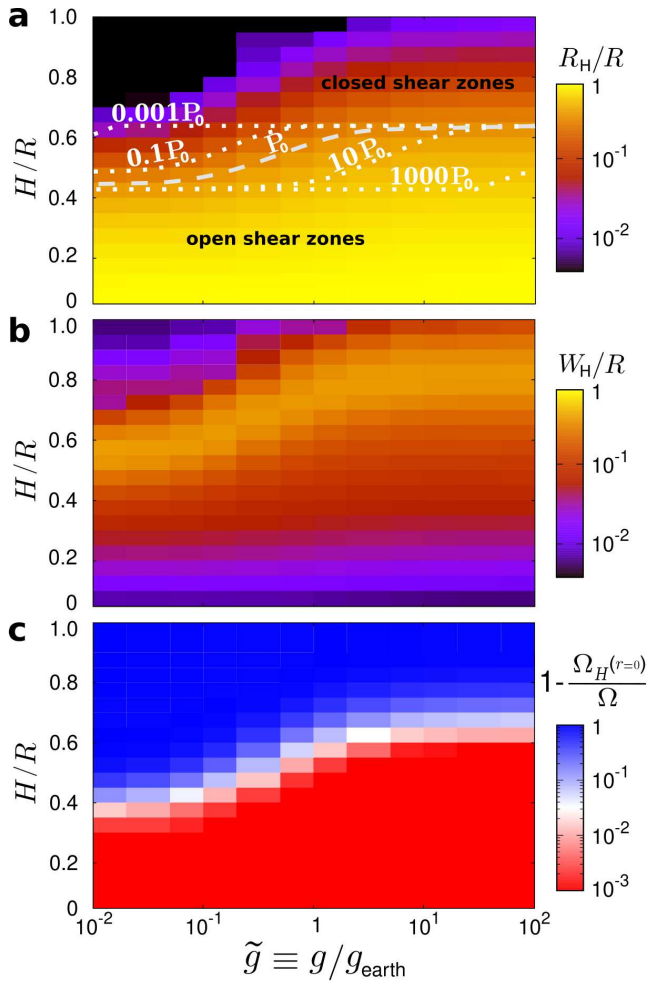

FIG. 3. Phase diagrams of the shear-zone position and width and the axial angular velocity at the top surface. **a**, Radial coordinate R_H of the center of shear zone (scaled by the radius R of the bottom disk) in the (g, H) space, for $P_{\rm ext}$=$P_\circ$. The dashed line denotes the threshold at which the open shear zone eventually reaches the rotation axis. The dotted lines represent the same threshold for other values of $P_{\rm ext}$. **b**, Scaled width of the shear zone at the top surface, W_H/R. **c**, Deviation of the axial angular velocity $\Omega_H(r{=}0)$ at the top surface from the driving rate Ω of the bottom disk.

the shear zone reaches the top surface for deeper layers as shown in Fig. 2. It can be also seen that the gravity pushes the open shear zones away from the axis of rotation and slightly reduces the extent of the zone. This is in contrast to the closed zones, where the gravity even increases the extent of the strain localization zone while pulls it towards the top surface.

We quantify the center of the shear zone at a given height h as the radial distance R_h at which the rate of the strain reaches its maximum, i.e. $\mathrm{d}\epsilon_{r\theta}/\mathrm{d}r|_{r=R_h}$=0. The width W_h is taken to be the variance of the shear rate $\mathrm{d}\Omega_h(r)/\mathrm{d}r$ around the peak at r=R_h. Figure 3 summarizes the behavior of the center position R_H, width W_H, and axial angular velocity $\Omega_H(r{=}0)$ at the top surface in the (g, H) space. The continuous transition from open to closed shear zone along the H-axis [21, 22] manifests itself e.g. in the abrupt change in the axial angular velocity from Ω to 0 (within the numerical accuracy of the measurements); see Fig. 3c. The gravity enhances the open shear zone regime to higher values of H. We can identify the transition from open to closed shear bands as, for example, when the shear localization region reaches the rotation axis. As shown in Fig. 3a, the transition line in the g-H phase diagram depends on the applied pressure $P_{\rm ext}$ but approaches a saturation level towards each extreme limit of g.

Universal characteristics of shear zones. The radial coordinate of the shear band at the top surface, R_H, monotonically increases with g for any choice of H and $P_{\rm ext}$; see Fig. 4a. Denoting the scaled gravity and pressure by $\widetilde{g}$≡$g/g_{\rm earth}$ and $\widetilde{P}$≡$P_{\rm ext}/P_\circ$, we introduce a dimensionless parameter λ=$\widetilde{g}/\widetilde{P}$ with which we can tune the relative strength of the gravity compared to the applied pressure. Interestingly, when plotting R_H versus λ in Fig. 4b, we achieve a striking data collapse for each filling height. The universal master curve at a given H suggests that to predict the flow profile as a function of gravity, one can instead use the inverse of the applied pressure as control parameter. To validate this hypothesis we carried out shear experiments in a modified Couette cell with a transparent plate on the top of the granular layer to apply pressure (see Fig. 5a and *Methods* section for details). Figure 4b shows that for several different filling heights the experimental data (obtained by varying the mass of the top plate) follow the master curves satisfactorily. Following the power-law scaling that was previously reported in cells without confining pressure [19, 20], we find that the entire data for all g, $P_{\rm ext}$, H, and R_H values lie on a universal curve

$$1-\frac{R_H}{R}=f(\lambda)\Big(\frac{H}{R}\Big)^{5/2}, \qquad (2)$$

where $f(\lambda)$ is a logistic function of $\ln\lambda$ (see inset of Fig. 4c):

$$f(\lambda)=a+\frac{b}{1+\mathrm{e}^{-(\ln\lambda+c)}}, \qquad (3)$$

with a, b, and c being fit parameters.

The width W_H of the shear zone at the top surface, shown in Fig. 4d, follows a scaling law

$$\frac{W_H}{R}\propto f(\lambda)\Big(\frac{H}{R}\Big)^{\beta}, \qquad (4)$$

with the exponent β=2/3, indicating that the extent of the shear zone grows faster than diffusively but slower than linearly with H. A similar growth exponent was observed in open surface shear experiments [19, 20]. There are, however, growing deviations from the scaling behavior as the filling height approaches the transition

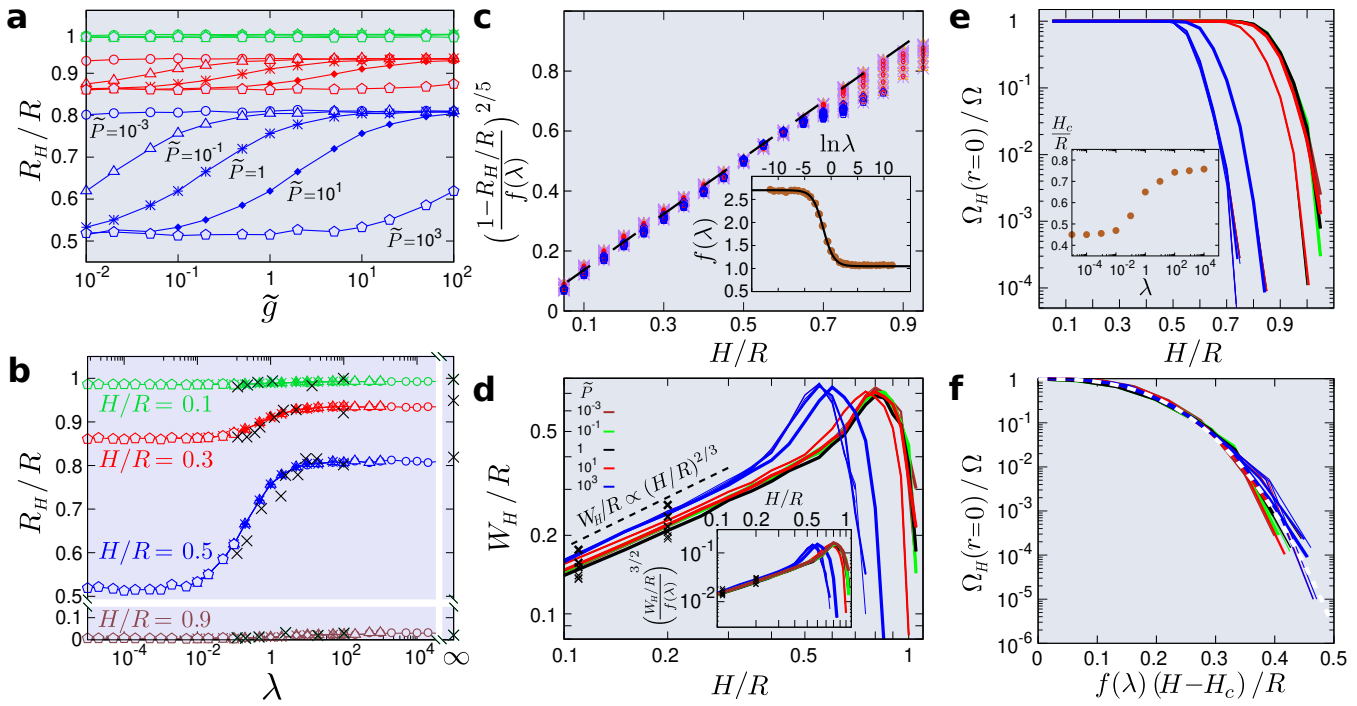

FIG. 4. Universal characteristics of shear zones. **a**, Radial coordinate of the shear band at the top surface, R_H, in terms of the scaled gravitational acceleration $\widetilde{g}\equiv g/g_{\rm earth}$. Different filling heights (applied pressures $\widetilde{P}\equiv P_{\rm ext}/P_\circ$) are indicated with different colors (symbols). **b**, R_H vs $\lambda=\widetilde{g}/\widetilde{P}$. The data shown in panel (**a**) collapses on a universal master curve for each H. Crosses represent experimental data. **c**, Scaled shear-zone position via equation (2) vs H/R. The dashed line indicates equality. Inset: $f(\lambda)$ vs $\ln\lambda$. The solid line is given by equation (3) with $a\simeq 2.7$, $b\simeq -1.7$, $c\simeq 1.5$. **d**, Width of the shear zone in terms of H for various $P_{\rm ext}$ (different colors) and g ($\widetilde{g}$ grows from 0.01 to 100 with increasing line thickness). Crosses represent experimental data at $H/R\simeq 0.11$, 0.20 (increasing symbol thickness with $P_{\rm ext}$). Inset: Collapse of the data onto a master curve using equation (4). **e**, Axial angular velocity at the top surface (scaled by the driving rate Ω of the bottom disk) as a function of H. Same colors and line thicknesses as in panel (**d**). The inset shows the variation of the cutoff height H_c with λ. **f**, Decay of $\Omega_H(r{=}0)$ with the scaled excess filling height $\widetilde{H}=f(\lambda)\,(H-H_c)/R$. The white dashed line is the scaling form given by equation (5).

threshold to the closed shear zones. While the exponent β remains unchanged, increasing g (or decreasing $P_{\rm ext}$) slightly decreases W_H. It was shown that gravity causes decreasing amplitude of grain displacement in signal propagation which slows down the dispersion of signal width [42]. The inset of Fig. 4d shows that a data collapse is achieved when rescaling according to equation (4) using a free fit to the logistic function (3).

In shallow layers, the top surface directly above the circular fault region rotates with the driving rate Ω of the bottom disk. As H increases, the angular velocity $\Omega_H(r)$ at the top surface gradually reduces during the crossover from open to closed shear zones. It can be seen from Fig. 4e that the cutoff height H_c (at which the axial angular velocity at the top surface $\Omega_H(r{=}0)$ starts decreasing) depends on $P_{\rm ext}$ and g. By subtracting H_c from the total height, we introduce a scaled excess filling height $\widetilde{H}{=}f(\lambda)\dfrac{H-H_c}{R}$. Then, the angular velocity data remarkably lie on a universal curve

$$\frac{\Omega_H(r{=}0)}{\Omega} = \exp\Big[-\big(\frac{\widetilde{H}}{\sigma}\big)^{\alpha}\Big] \qquad (5)$$

(with $\alpha\simeq 2.8$ and σ being the standard deviation), which extends over several orders of magnitude.

While the scaling relations (2),(4),(5) for the top-surface characteristics enable one to predict the influence of the gravity on the surface flow profile, the variational approach accurately determines the shear zone path inside the bulk as well. As the final experimental validation of the numerical approach, we first numerically obtain the center position of the shear band in the bulk for a given H and $P_{\rm ext}$ and several choices of g. To achieve the corresponding values of λ in experiments, we adjust $P_{\rm ext}$ (i.e. the mass of the top plate). To be able to visualize the bulk flow profile, we initially create straight lines of colored beads buried at several heights in the bulk and observe the created patterns after shearing by removing the upper layers of grains (see Fig. 5a). The numerical and experimental results of R_h versus h are compared

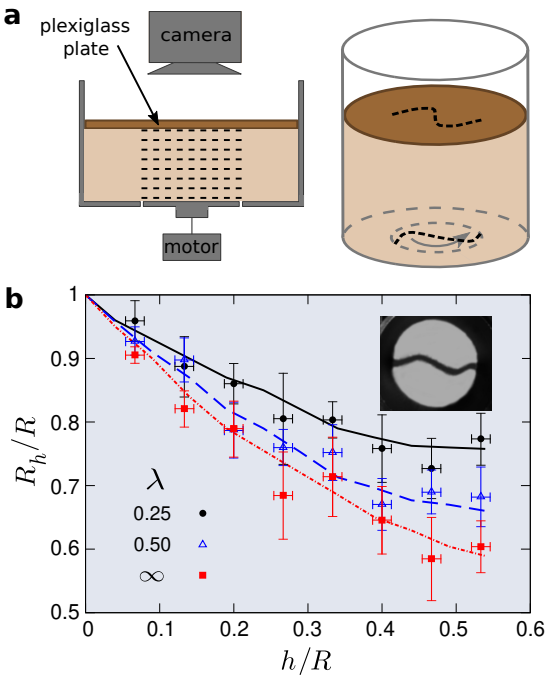

FIG. 5. Sketch of the experimental setup and evolution of the patterns within the bulk. **a**, The split-bottom Couette cell. (left) The dashed lines indicate the heights where the initially straight lines of colored beads were created. (right) Schematic of the resulting lower and upper patterns after shearing. **b**, Position R_h of the shear band at height h within the bulk, for H/R=0.55 and different values of λ. The lines (symbols) represent numerical (experimental) data. To achieve the indicated values of λ in experiments we apply $P_{\rm ext}/P_\circ$=4.0, 2.0, or 0 (corresponding to λ=0.25, 0.50, ∞). In simulations we use $g/g_{\rm earth}$=0.25, 0.5, 1 and $P_{\rm ext}/P_\circ$=1, 1, 0. The inset shows a typical pattern of colored beads within the bulk, obtained experimentally.

in Fig. 5b; the agreement is excellent, without any adjustable parameter.

In conclusion, we studied the role of gravity on strain localization in slowly sheared granular materials. The variational approach for minimization of energy dissipation is computationally a cheaper technique even compared to efficient DEM tools for large-scale granular simulations [43, 44] and can be extended to more complex geometries. We obtained universal scaling laws describing the characteristics of the surface flow profile, which opens the possibility of predicting the shear flow of granular matter in varying gravitational environments. Since shear zones mark the regions where energy dissipation and catastrophic material failures occur, our results are of particular relevance for science and engineering challenges associated with planetary and asteroid exploration programs in the coming years and decades.

METHODS

Variational approach. In order to perform the numerical simulations based on the variational minimization principle, we note that the cylindrical symmetry reduces the problem to an effective 2D one. A square lattice with the lattice unit being equal to the grain size d is considered. Here, the results for d/R=10^{-2} are presented. An instantaneous shear band is obtained via equation (1), which has one lattice unit width. Next, the local material strength along the shear band and in its neighborhood are randomly updated following the probability distribution $P(\mu^{\rm eff})$ reported in [37]. By repeating the procedure, an ensemble of shear bands are obtained from which the characteristics of the shear zone are deduced.

Experimental setup. Our experimental setup is similar in spirit to the modified Couette cell used in previous granular shear experiments [19, 21, 22], but with an additional plexiglass plate laid on top of the granular layer to generate pressure on the sample; see Fig. 5a. The bottom disk with radius R=45 or 75 mm is rotated at small angular velocity $\Omega\simeq$0.1 rad/s to avoid rate-dependent stresses [11]. The mass of the top plate ranges from 50 to 5000 gr and glass beads with the average diameter of 0.5 to 5 mm with size polydispersity of about 15% are used to prevent ordering of grains near walls [13, 45]. The gap size at the split is less than 400 μm so that no particle can escape. The surface flow is monitored from above by a fast CCD camera with pixel resolution 70 μm and frame rate 30 s^{-1}. The experiments are carried with and without the top plate. To obtain the flow profile, particle image velocimetry method is used to determine the average angular cross-correlation function for successive frames. The axial angular velocity at the top surface is extracted by averaging the angular velocities within a small circle of radius 5 mm around the cylinder axis.

JT acknowledges support by Hungarian National Research, Development and Innovation Office (NKFIH), under Grant No. OTKA K 116036, by the BME IE-VIZTKP2020.

* shaebani@lusi.uni-sb.de

[1] D. Hestroffer, P. Sánchez, L. Staron, A. C. Bagatin, S. Eggl, W. Losert, N. Murdoch, E. Opsomer, F. Radjai, D. C. Richardson, et al., Astron. Astrophys. Rev. **27**, 6 (2019).
[2] K. Harth, T. Trittel, S. Wegner, and R. Stannarius, Phys. Rev. Lett. **120**, 214301 (2018).
[3] N. Murdoch, B. Rozitis, K. Nordstrom, S. F. Green, P. Michel, T.-L. de Lophem, and W. Losert, Phys. Rev. Lett. **110**, 018307 (2013).
[4] A. Sack, M. Heckel, J. E. Kollmer, and T. Pöschel, Granular Matter **17**, 73 (2015).
[5] H. Katsuragi and J. Blum, Phys. Rev. Lett. **121**, 208001

(2018).
[6] M. Noirhomme, A. Cazaubiel, A. Darras, E. Falcon, D. Fischer, Y. Garrabos, C. Lecoutre-Chabot, S. Merminod, E. Opsomer, F. Palencia, et al., EPL **123**, 14003 (2018).
[7] N. Murdoch, B. Rozitis, S. F. Green, T.-L. de Lophem, P. Michel, and W. Losert, Granular Matter **15**, 129 (2013).
[8] D. R. Scott, Nature **381**, 592 (1996).
[9] A. Daerr and S. Douady, Nature **399**, 241 (1999).
[10] M. Oda and H. Kazama, Géotechnique **48**, 465 (1998).
[11] R. R. Hartley and R. P. Behringer, Nature **421**, 928 (2003).
[12] W. Losert, L. Bocquet, T. C. Lubensky, and J. P. Gollub, Phys. Rev. Lett. **85**, 1428 (2000).
[13] D. M. Mueth, G. F. Debregeas, G. S. Karczmar, P. J. Eng, S. R. Nagel, and H. M. Jaeger, Nature **406**, 385 (2000).
[14] J. E. Kollmer, T. Shreve, J. Claussen, S. Gerth, M. Salamon, N. Uhlmann, M. Schröter, and T. Pöschel, Phys. Rev. Lett. **125**, 048001 (2020).
[15] P. Schall and M. van Hecke, Annu. Rev. Fluid Mech. **42**, 67 (2010).
[16] R. Moosavi, M. R. Shaebani, M. Maleki, J. Török, D. E. Wolf, and W. Losert, Phys. Rev. Lett. **111**, 148301 (2013).
[17] H. A. Knudsen and J. Bergli, Phys. Rev. Lett. **103**, 108301 (2009).
[18] T. Unger, J. Török, J. Kertész, and D. E. Wolf, Phys. Rev. Lett. **92**, 214301 (2004).
[19] D. Fenistein, J. W. van de Meent, and M. van Hecke, Phys. Rev. Lett. **92**, 094301 (2004).
[20] D. Fenistein and M. van Hecke, Nature **425**, 256 (2003).
[21] X. Cheng, J. B. Lechman, A. Fernandez-Barbero, G. S. Grest, H. M. Jaeger, G. S. Karczmar, M. E. Möbius, and S. R. Nagel, Phys. Rev. Lett. **96**, 038001 (2006).
[22] D. Fenistein, J.-W. van de Meent, and M. van Hecke, Phys. Rev. Lett. **96**, 118001 (2006).
[23] T. I. Riikilä, J. I. Pylväinen, and J. Åström, Phys. Rev. Lett. **119**, 255501 (2017).
[24] J. Török, T. Unger, J. Kertész, and D. E. Wolf, Phys. Rev. E **75**, 011305 (2007).
[25] A. Singh, V. Magnanimo, K. Saitoh, and S. Luding, New J. Phys. **17**, 043028 (2015).
[26] M. R. Shaebani, T. Unger, and J. Kertész, Phys. Rev. E **76**, 030301 (2007).
[27] C. Goldenberg and I. Goldhirsch, Nature **435**, 188 (2005).
[28] G. D. R. MiDi, Eur. Phys. J. E **14**, 341 (2004).
[29] M. R. Shaebani, T. Unger, and J. Kertész, Phys. Rev. E **79**, 052302 (2009).
[30] L. Onsager, Phys. Rev. **37**, 405 (1931).
[31] L. Onsager, Phys. Rev. **38**, 2265 (1931).
[32] R. Baker and M. Garber, Géotechnique **28**, 395 (1978).
[33] T. Unger, Phys. Rev. Lett. **98**, 018301 (2007).
[34] B. Szabó, J. Török, E. Somfai, S. Wegner, R. Stannarius, A. Böse, G. Rose, F. Angenstein, and T. Börzsönyi, Phys. Rev. E **90**, 032205 (2014).
[35] T. Börzsönyi, T. Unger, and B. Szabó, Phys. Rev. E **80**, 060302 (2009).
[36] M. R. Shaebani, T. Unger, and J. Kertész, Int. J. Mod. Phys. C **20**, 847 (2009).
[37] M. R. Shaebani, T. Unger, and J. Kertész, Phys. Rev. E **78**, 011308 (2008).
[38] M. M. Bandi, P. Das, O. Gendelman, H. G. E. Hentschel, and I. Procaccia, Granular Matter **21**, 40 (2019).
[39] M. Kobayakawa, S. Miyai, T. Tsuji, and T. Tanaka, Phys. Rev. E **98**, 052907 (2018).
[40] M. R. Shaebani, J. Boberski, and D. E. Wolf, Granular Matter **14**, 265 (2012).
[41] P. Das, H. G. E. Hentschel, and I. Procaccia, Phys. Rev. E **99**, 050902 (2019).
[42] J. Hong and A. Xu, Phys. Rev. E **63**, 061310 (2001).
[43] Z. Shojaaee, M. R. Shaebani, L. Brendel, J. Török, and D. E. Wolf, J. Comput. Phys. **231**, 612 (2012).
[44] C. Kloss, C. Goniva, A. Hager, S. Amberger, and S. Pirker, Prog. Comput. Fluid Dyn. **12**, 140 (2012), URL `https://www.cfdem.com/liggghts-open-source-code`.
[45] G. Chambon, J. Schmittbuhl, A. Corfdir, J. P. Vilotte, and S. Roux, Phys. Rev. E **68**, 011304 (2003).